CHAPTER 6

Approaching Control Based on a Movable Platform

The approach control of a tethered space robot system is a very challenging research issue that involves two research areas. One is the noncooperative target detection and tracking, and the other is the rendezvous control using the space tether. In the area of noncooperative target detection and tracking, Du et al. studied the pose measurement problem presented by a large noncooperative satellite based on two collaborative cameras [1]. A nonlinear and recursive identification mechanism in a motion-based detection and tracking algorithm is presented in Doulamis [2]. Thienel et al. designed a nonlinear approach for estimating the body rates of a noncooperative target vehicle and coupled the estimation to a tracking control scheme [3]. Under the assumption that the noncooperative target has been detected and measured by the visual perception system of a TSR, this chapter focuses on the rendezvous control using the space tether. In this area, the tether-mediated orbital rendezvous between the tether tip and the space shuttle was first discussed by Carroll [4]. Several years later, Carroll provided a preliminary design for a tether transport facility capable of providing between 0.6 and 1.2 km/s velocity increments to payloads [5]. Stuart originally considered the in-plane cooperative tether-mediated rendezvous between a free-flying spacecraft and the tether tip by combining tether reeling with thrusters on the tether tip [6]. More recently, Blanksby and Trivailo proposed a method to realize a gentle rendezvous by the tension controller [7]. Westerhoff discussed a linear control strategy to minimize errors in rendezvous for a spinning momentum-exchange system, which assumed that the tether is reasonably close to the desired rendezvous position [8]. Williams studied payload capture problems and examined the influence of thermomechanical and tether flexibility effects [9–12]. However, most of the previous studies have focused on the dynamic and control problem of a long-tether system, which is known as the tethered space satellite system (TSS) [13–15]. Rather than TSS, this chapter proposes a TSR for the on-orbit capture task. The space tether of TSR is only a few hundred meters long, which is much

https://doi.org/10.1016/B978-0-12-812309-6.00006-3

shorter than the traditional TSS. The tether deployment depends on ejection velocity instead of the gravity gradient, and the whole capture operation only takes a matter of minutes. The short dimensions and different deployment procedure distinguish TSR from the traditional TSS. Furthermore, the relative states between the target and TSR are much more important in the studies of the TSR. Therefore the previous achievements are not suitable for TSR. In studies of TSR, Mankala and Agrawal examined dynamic modeling and simulation [16]. Nakamura discussed the collaborative control method [17], but did not consider the attitude disturbances and relative motions among the platform, tether, robot, and target. The multibody relative motion should not be ignored because of its importance to the direction of tension and the approach instruction. With consideration for the relative motions among platform, target, and gripper, the approach control problem of the TSR is studied in this chapter.

6.1 APPROACH DYNAMIC MODEL

A TSR is a typical rigid-flexible combination system. The tether modeling is more complex, which has been investigated by numerous researchers. In this chapter, the traditional bead model is used to represent the space tether. The tether is assumed to be a series of point masses connected by *i* massless springs of constant undeformed lengths, which can describe some characteristics of the tether such as mass, elasticity, flexibility, and slack. The bead model of a TSR is showed in Fig. 6.1.

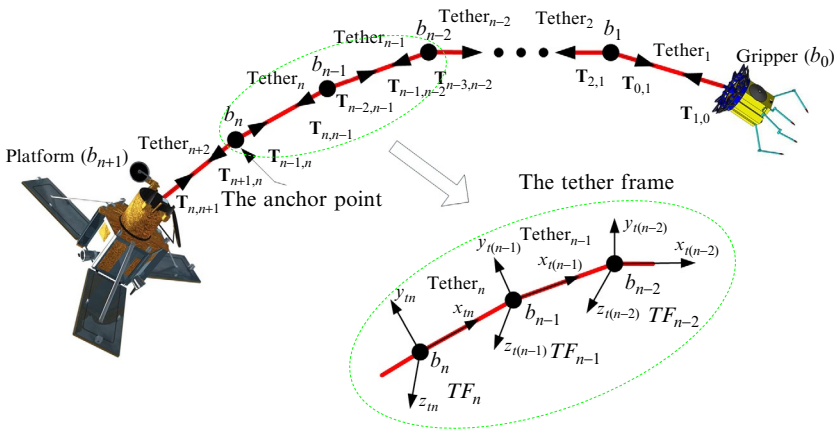

Fig. 6.1 Bead model.

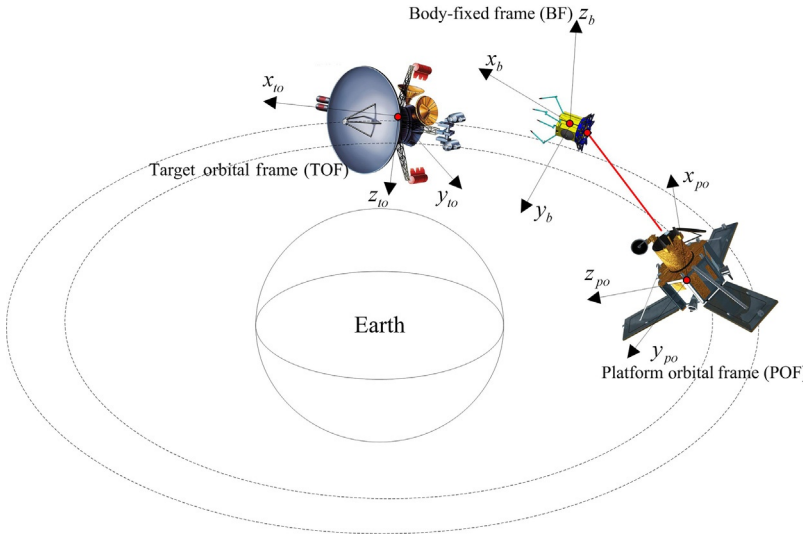

Fig. 6.2 Reference frames for the rendezvous model of a TSR.

There are $n+1$ tether coordinate systems (Tether Frame, TF_i, $i=1,\ldots,n+1$) in the bead model. Also, the target orbital frame (TOF), platform orbital frame (POF), and body-fixed frame (BF) are used as the reference frames in the approach modeling of TSR (Fig. 6.2). TOF is formed with its origin in the mass center of the target. The three axes are defined by unit vectors $(\boldsymbol{x}_{to}, \boldsymbol{y}_{to}, \boldsymbol{z}_{to})$, where $\boldsymbol{z}_{to}$ is directed from the center of Earth to the mass center of the target and represents the system local vertical, $\boldsymbol{y}_{to}$ is the orbital angular momentum unit vector, and $\boldsymbol{x}_{to}$ completes the frame following the right-hand principle. POF $(\boldsymbol{x}_{po}, \boldsymbol{y}_{po}, \boldsymbol{z}_{po})$ is similar to TOF, and its origin is the mass center of the platform. BF $(\boldsymbol{x}_b, \boldsymbol{y}_b, \boldsymbol{z}_b)$ is the principal axis frame of the gripper, which indicates that the three axes are also the principal axes of system inertia. $TF_i(\boldsymbol{x}_{ti}, \boldsymbol{y}_{ti}, \boldsymbol{z}_{ti})$ is set with its origin at b_i, where $\boldsymbol{x}_{ti}$ is directed from b_i to b_{i-1} along the tether, $\boldsymbol{y}_{ti}$ is in the target orbit plane and is perpendicular to $\boldsymbol{x}_{ti}$, and $\boldsymbol{z}_{ti}$ completes the frame following the right-hand principle.

As shown in Fig. 6.3, there are eight thrusters, a reaction wheel, and a tether. The attitude is stabilized by the thrusters and the reaction wheel. In the channels around directions $\boldsymbol{y}_b$ and $\boldsymbol{z}_b$, the tether tension is the principal interference except for the release disturbance. The control moments should be supplied by a couple of the thrust. The control moment around $\boldsymbol{x}_b$ direction is supplied by the reaction wheel. In this channel, the interference by

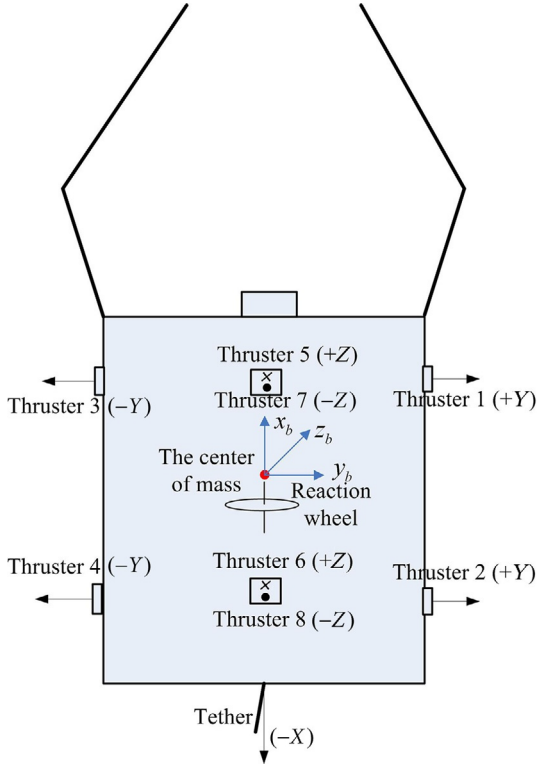

Fig. 6.3 Configuration of actuators.

the tether tension should be neglected, for the tie-point of the tether to the gripper is on the x-axes. The main interference is the release disturbance, which should have been previously estimated. Therefore it is assumed that the reaction wheel should not be saturated in an approach. The momentum should be unloaded before the release for another mission. The TSR is controlled by thrusters and the tether to follow the trajectory. Thrusters should supply the control force along the direction $-\boldsymbol{y}_b$, $+\boldsymbol{y}_b$, $-\boldsymbol{z}_b$, and $+\boldsymbol{z}_b$. Along the $-\boldsymbol{x}_b$ direction, the tether can supply almost all of the control force. For the release velocity, the control force along $+\boldsymbol{x}_b$ direction should not be necessary. The assignment of actuators is shown in Table 6.1.

6.1.1 The Attitude Model

The attitude of the gripper should be maintained in the approach stage of a TSR. Due to the presence of tension and other disturbances, the reaction wheel and the thrusters should be used to maintain the attitude stabilized. If the attitude instruction is stabilizing the attitude angle between BF and

Table 6.1 Assignment of the actuators

Forces and moments	Actuators
$+F_{sx}/-F_{sx}$	Not necessity/the tether
$+F_{sy}/-F_{sy}$	Thrusters: 1 and 2/3 and 4
$+F_{sz}/-F_{sz}$	Thrusters: 5 and 6/7 and 8
$+T_{cx}/-T_{cx}$	The reaction wheel
$+T_{cy}/-T_{cy}$	The couple of thrusters: 6 and 7/5 and 8
$+T_{cz}/-T_{cz}$	The couple of thrusters: 2 and 3/1 and 4

TF_1, the tension moment may be the restoring moment around the axes y_t and z_t.

The traditional attitude control model of the reaction wheel and thrusters is:

$$\begin{cases} \boldsymbol{I}\dot{\boldsymbol{\omega}} + [\boldsymbol{\omega}\times](\boldsymbol{I}\boldsymbol{\omega} + \boldsymbol{h}) = -\dot{\boldsymbol{h}} + \boldsymbol{T}_c + \boldsymbol{T}_t + \boldsymbol{T}_d \\ \dot{\boldsymbol{q}} = 0.5[\boldsymbol{q}\times]\boldsymbol{\omega} \end{cases} \tag{6.1}$$

where

$$[\boldsymbol{\omega}\times] = \begin{bmatrix} 0 & -\omega_z & \omega_y \\ \omega_z & 0 & -\omega_x \\ -\omega_y & \omega_x & 0 \end{bmatrix},$$

$$[\boldsymbol{q}\times] = \begin{bmatrix} -q_1 & -q_2 & -q_3 \\ q_4 & -q_3 & q_2 \\ q_3 & q_4 & -q_1 \\ -q_2 & q_1 & q_4 \end{bmatrix},$$

$\boldsymbol{\omega} = [\omega_x \ \ \omega_y \ \ \omega_z]^{\mathrm{T}}$ is the angular velocity of the gripper; $\boldsymbol{I} = \mathrm{diag}(I_x, I_y, I_z)$ is the inertia matrix; $\boldsymbol{q} = [q_1, q_2, q_3, q_4]$ is the relative attitude quaternion of BF and TF_1; $\boldsymbol{h}$ is the angular moment; $\boldsymbol{T}_c$ is the control moment; and $\boldsymbol{T}_t$ and $\boldsymbol{T}_d$ represent the tension moment and the other interferential moment, respectively. Also, due to the convenience of expression and measurement, the output attitude is expressed as a form of Tait-Bryan angles instead of quaternion in this chapter. The derivation of Tait-Bryan angles (roll, pitch, yaw error $[\phi, \theta, \psi]^{\mathrm{T}}$) from the attitude quaternion is as follows [18]:

$$\begin{bmatrix} \phi \\ \theta \\ \psi \end{bmatrix} = \begin{bmatrix} \arctan\left(\dfrac{2(q_1q_4 + q_2q_3)}{1 - 2(q_1^2 + q_2^2)}\right) \\ \arcsin\left(2(q_4q_2 - q_3q_1)\right) \\ \arctan\left(\dfrac{2(q_4q_3 + q_1q_2)}{1 - 2(q_2^2 + q_3^2)}\right) \end{bmatrix} \tag{6.2}$$

6.1.2 The Trajectory Model

The relative motion of the platform, gripper, and target is the core of the TSR trajectory model, which significantly differs from the modeling of the TSS. The target satellite is assumed to work along an unperturbed circular orbit. We use the well-known Hill equation to describe the gripper, tether, and platform dynamic modeling for the approach stage of the TSR. Also, the distance between the TSR and the target is extremely small compared to the orbital radius of the target. The higher order nonlinear terms of the Hill equation should be neglected. Then, a reduction should be used in this chapter.

Define the unit vector of TOF as $(\boldsymbol{i},\boldsymbol{j},\boldsymbol{k})$, and the position and acceleration of gripper as $\boldsymbol{r}_s$ and $\boldsymbol{a}_s$. The position and acceleration of platform are $\boldsymbol{r}_p$ and $\boldsymbol{a}_p$. The position and acceleration of the bead b_i are $\boldsymbol{r}_{t,i}$ and $\boldsymbol{a}_{t,i}$. From Fig. 6.3, $\boldsymbol{r}_s$ and $\boldsymbol{r}_p$ should be expressed as $\boldsymbol{r}_{t,0}$ and $\boldsymbol{r}_{t,n+1}$.

The tether coordinate system TF_i is represented as:

$$\begin{cases} \boldsymbol{x}_{t,i} = (\boldsymbol{r}_{t,i-1} - \boldsymbol{r}_{t,i})/|\boldsymbol{r}_{t,i-1} - \boldsymbol{r}_{t,i}| \\ \boldsymbol{y}_{t,i} = \boldsymbol{x}_{t,i} - (\boldsymbol{x}_{t,i} \cdot \boldsymbol{j})\boldsymbol{j} \\ \boldsymbol{z}_{t,i} = \boldsymbol{x}_{t,i} \times \boldsymbol{y}_{t,i} \end{cases} \tag{6.3}$$

From the rotation matrix from TF_i to TOF, we have:

$$\begin{cases} \boldsymbol{A}_{\boldsymbol{T}_i,\boldsymbol{O}} = \boldsymbol{f}_{\boldsymbol{T}_i,\boldsymbol{O}}(\boldsymbol{r}_s, \boldsymbol{r}_{t,i}) \quad i = 1,\ldots,n \\ \boldsymbol{A}_{\boldsymbol{T}_{n+1},\boldsymbol{O}} = \boldsymbol{f}_{\boldsymbol{T}_i,\boldsymbol{O}}(\boldsymbol{r}_{t,n}, \boldsymbol{r}_p) \end{cases} \tag{6.4}$$

The rotation matrix from BF to TF_1 is represented as:

$$\boldsymbol{A}_{\boldsymbol{B},\boldsymbol{T}_1} = \boldsymbol{f}_{\boldsymbol{B},\boldsymbol{T}_1}(q_1, q_2, q_3, q_4) \tag{6.5}$$

The acceleration of gripper, platform and bead b_i can then be derived in TOF:

$$\begin{cases} \boldsymbol{a}_s = \begin{bmatrix} a_{sx} \\ a_{sy} \\ a_{sz} \end{bmatrix} = \dfrac{1}{m_s}\boldsymbol{A}_{\boldsymbol{T}_1,\boldsymbol{O}}\left(\begin{bmatrix} T_{1,0} \\ 0 \\ 0 \end{bmatrix} + \boldsymbol{A}_{\boldsymbol{B},\boldsymbol{T}_1}\begin{bmatrix} F_{sx} \\ F_{sy} \\ F_{sz} \end{bmatrix}\right) \\ \boldsymbol{a}_p = \begin{bmatrix} a_{px} \\ a_{py} \\ a_{pz} \end{bmatrix} = \dfrac{1}{m_p}\left(\boldsymbol{A}_{\boldsymbol{T}_{n+1},\boldsymbol{O}}\begin{bmatrix} T_{n,n+1} \\ 0 \\ 0 \end{bmatrix} + \begin{bmatrix} F_{px} \\ F_{py} \\ F_{pz} \end{bmatrix}\right) \end{cases} \tag{6.6}$$

$$\boldsymbol{a}_{t,i}=\begin{bmatrix}a_{t,ix}\\a_{t,iy}\\a_{t,iz}\end{bmatrix}=\frac{1}{m_{b_i}}\left(\boldsymbol{A}_{\boldsymbol{T}_{i+1},\boldsymbol{O}}\begin{bmatrix}T_{i+1,i}\\0\\0\end{bmatrix}+\boldsymbol{A}_{\boldsymbol{T}_i,\boldsymbol{O}}\begin{bmatrix}T_{i-1,i}\\0\\0\end{bmatrix}\right),\quad i=1,\ldots,n \tag{6.7}$$

where m_s, m_p, and m_{b_i} are the respective masses of the gripper, platform, and bead b_i; F_{sx}, F_{sy}, and F_{sz} are the thrusts of gripper along the x-, y-, and z-axes of BF, respectively; $T_{i,i+1}=-T_{i+1,i}$ $(i=0,\ldots,n)$ is the tether tension along the ith link ("tether i"); F_{px}, F_{py}, F_{pz} are the control thrusts of platform at TOF.

The tether tension can be derived:

$$\begin{cases}T_{i-1,i}=\begin{cases}EA(\varepsilon_i+c\dot{\varepsilon}_i) & \varepsilon_i\geq 0\\ 0 & \varepsilon_i<0\end{cases} & i=1,\ldots,n\\ \varepsilon_i=\dfrac{|\boldsymbol{r}_{t,i}-\boldsymbol{r}_{t,i-1}|-l_i}{l_i}\end{cases} \tag{6.8}$$

where l_i is the original length of the tether i, E is Young's modulus, A is the area of cross-section and EA is the tether's longitudinal stiffness.

Contrast to the ith elastic link $(i=1,\ldots,n)$, the $(n+1)$th link of the tether is assumed to be inelastic. The stored tether is deployed by varying the length of the $(n+1)$th link. During the deployment, the new bead appears and a new anchor point is defined when the length of $(n+1)$th link is larger than a designed constant. $T_{n,n+1}$ is the deployment force of the platform, which can be represented by T_{tp}.

The trajectory model for the approach stage is derived by using the Hill equation in TOF.

$$\begin{cases}\begin{bmatrix}\ddot{x}_s-2\omega\dot{z}_s\\ \ddot{y}_s+\omega^2\gamma_s\\ \ddot{z}_s+2\omega\dot{x}_s-3\omega^2 z_s\end{bmatrix}=\dfrac{1}{m_s}\boldsymbol{A}_{\boldsymbol{T}_1,\boldsymbol{O}}\left(\begin{bmatrix}T_{1,0}\\0\\0\end{bmatrix}+\boldsymbol{A}_{\boldsymbol{B},\boldsymbol{T}_1}\begin{bmatrix}F_{sx}\\F_{sy}\\F_{sz}\end{bmatrix}\right)\\ \begin{bmatrix}\ddot{x}_p-2\omega\dot{z}_p\\ \ddot{y}_p+\omega^2\gamma_p\\ \ddot{z}_p+2\omega\dot{x}_p-3\omega^2 z_p\end{bmatrix}=\dfrac{1}{m_p}\left(\boldsymbol{A}_{\boldsymbol{T}_{n+1},\boldsymbol{O}}\begin{bmatrix}T_{n,n+1}\\0\\0\end{bmatrix}+\begin{bmatrix}F_{px}\\F_{py}\\F_{pz}\end{bmatrix}\right)\\ \begin{bmatrix}\ddot{x}_{t,i}-2\omega\dot{z}_{t,i}\\ \ddot{y}_{t,i}+\omega^2\gamma_{t,i}\\ \ddot{z}_{t,i}+2\omega\dot{x}_{t,i}-3\omega^2 z_{t,i}\end{bmatrix}=\dfrac{1}{m_{b_i}}\left(\boldsymbol{A}_{\boldsymbol{T}_{i+1},\boldsymbol{O}}\begin{bmatrix}T_{i+1,i}\\0\\0\end{bmatrix}+\boldsymbol{A}_{\boldsymbol{T}_i,\boldsymbol{O}}\begin{bmatrix}T_{i-1,i}\\0\\0\end{bmatrix}\right)\quad i=1,\ldots,n\end{cases} \tag{6.9}$$

where ω is the orbit angular velocity of the target.

6.2 APPROACH CONTROL STRATEGY

If the attitude can be stabilized by the reaction wheel or other actuators, the attitude will exert a slight influence on the trajectory control. Then, the control strategy for the attitude and orbit motion is designed, respectively. In the end, the complete control strategy will be validated in the complex coupling model. The approach control scheme is shown in Fig. 6.4, which contains the open-loop optimal trajectory controller, the close-loop adaptive controller, and the attitude controller.

6.2.1 Open-Loop Trajectory Optimization

If the attitude of gripper can be well controlled, the influence of attitude can be ignored. However, the trajectory model is still too complex to design the controller. In the approach stage, the gripper approaches the target by the initial release velocity and the tether is short and deployed in a passive mode. The tension should not be too small to reduce the disturbance for the gripper. Therefore the influence of tether mass, elasticity, and flexibility are weak. The tether can be simplified as an elongated, straight, and massless rigid body. The approach trajectory model of the TSR should be derived:

$$\begin{cases} \begin{bmatrix} \ddot{x}_s - 2\omega\dot{z}_s \\ \ddot{y}_s + \omega^2 y_s \\ \ddot{z}_s + 2\omega\dot{x}_s - 3\omega^2 z_s \end{bmatrix} = \dfrac{1}{m_s}\boldsymbol{A_{TO}}\left(\begin{bmatrix} -T_{tp} \\ 0 \\ 0 \end{bmatrix} + \boldsymbol{A_{BT}}\begin{bmatrix} F_{sx} \\ F_{sy} \\ F_{sz} \end{bmatrix}\right) \\ \begin{bmatrix} \ddot{x}_p - 2\omega\dot{z}_p \\ \ddot{y}_p + \omega^2 y_p \\ \ddot{z}_p + 2\omega\dot{x}_p - 3\omega^2 z_p \end{bmatrix} = \dfrac{1}{m_p}\left(\boldsymbol{A_{TO}}\begin{bmatrix} T_{tp} \\ 0 \\ 0 \end{bmatrix} + \begin{bmatrix} F_{px} \\ F_{py} \\ F_{pz} \end{bmatrix}\right) \end{cases} \tag{6.10}$$

If the attitude of the gripper can be stabilized by the reaction wheel and the thrusters, $\boldsymbol{A_{BT}}$ will keep constant. Also, the thrusters of the platform should not be used for the trajectory control and maneuvering in the approach stage. The approach trajectory model can be rewritten as follows:

$$\dot{\boldsymbol{X}} = \boldsymbol{f_r}(\boldsymbol{X}, \boldsymbol{U}) \tag{6.11}$$

where $\boldsymbol{X} = \left[x_s, \dot{x}_s, y_s, \dot{y}_s, z_s, \dot{z}_s, x_p, \dot{x}_p, y_p, \dot{y}_p, z_p, \dot{z}_p\right]^{\mathrm{T}}$ are the system state variables; $\boldsymbol{U} = \left[T_{tp}, F_{sx}, F_{sy}, F_{sz}\right]^{\mathrm{T}}$ are the system control variables; T_{tp} is the deployment force of the platform, which should be actualized by the friction between the tether and the tether control system; F_{sx}, F_{sy}, and F_{sz}

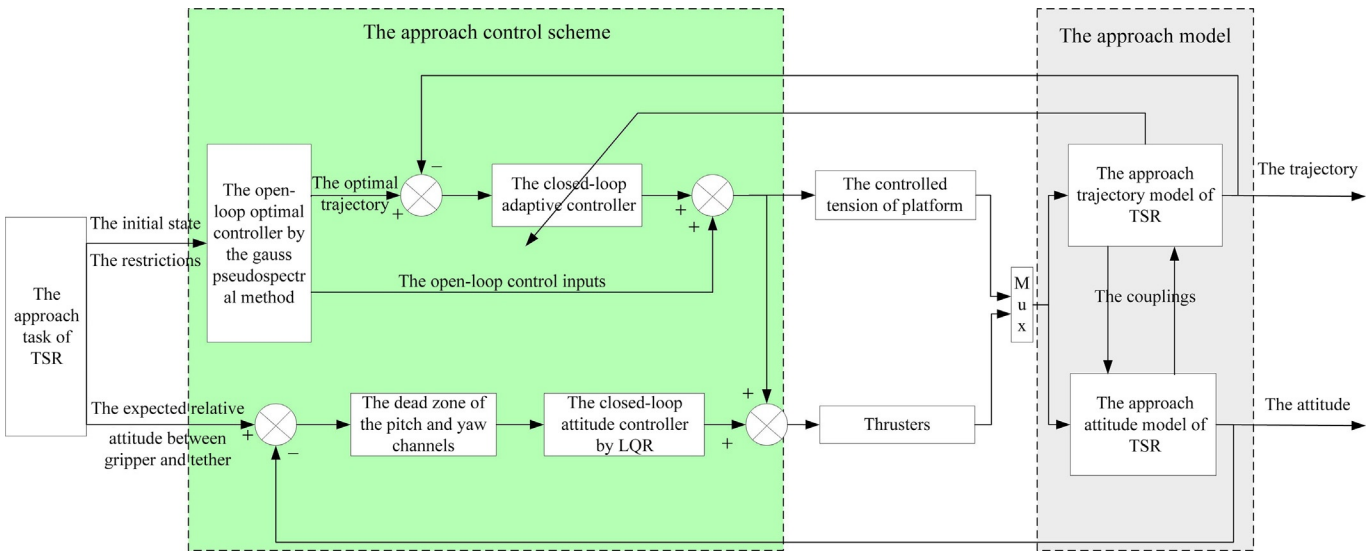

Fig. 6.4 Approach control scheme.

are the thrusts of gripper; To save the propellant and reduce the number of thrusters, F_{sx} is usually zero in the coordinated approach control scheme.

The objective of this section is to find a physically realizable trajectory that guides the gripper from a given initial state to a fixed terminal state. The problem is well defined mathematically as a two-point boundary value problem. In general, there may be a finite number of trajectories that satisfy the boundary conditions. Therefore the numerical solution is not necessarily unique. Despite the numerous possible measures for defining an optimal trajectory, the trajectory which satisfies the boundary conditions and minimizes the integral square of the thrust is defined as optimal in this chapter, which can reflect the advantage of coordinated control with tension and thrust.

In this chapter, the optimal control problem can be described as follows: Find the state-control pair $\{\boldsymbol{X}(t), \boldsymbol{U}(t)\}$ over the time interval $[t_0, t_f]$ that minimizes the performance index:

$$J = \int_{t_0}^{t_f} \left(F_{sy}^2 + F_{sz}^2 \right) dt \tag{6.12}$$

Subject to the nonlinear state equations given by Eq. (6.11), the initial and final boundary conditions

$$\boldsymbol{X}_{t_0} = \left[x_{s0}, \dot{x}_{s0}, y_{s0}, \dot{y}_{s0}, z_{s0}, \dot{z}_{s0}, x_{p0}, \dot{x}_{p0}, y_{p0}, \dot{y}_{p0}, z_{p0}, \dot{z}_{p0} \right]^{\mathrm{T}} \tag{6.13}$$

$$\mathbf{X}_{t_f} = \left[x_{sf}, \dot{x}_{sf}, y_{sf}, \dot{y}_{sf}, z_{sf}, \dot{z}_{sf}, x_{pf}, \dot{x}_{pf}, y_{pf}, \dot{y}_{pf}, z_{pf}, \dot{z}_{pf} \right]^{T} \tag{6.14}$$

and the box constraints

$$\boldsymbol{U}_{\min} \leq \boldsymbol{U}(t) = \left[T_{tp}, F_{sx}, F_{sy}, F_{sz} \right]^{T} \leq \boldsymbol{U}_{\max} \tag{6.15}$$

where $\boldsymbol{U}_{\min}$ and $\boldsymbol{U}_{\max}$ are the lower and upper bounds of control inputs.

The optimal control problem is generally difficult to be solved by using standard approaches. The pseudospectral method parameterizes the state and control variables by orthogonal polynomials (e.g., Legendre and Chebyschev). In this method, the dynamics are approximated at various quadrature points, such as the Legendre-Gauss, Legendre-Gauss-Radau, and Legendre-Gauss-Lobatto points. The use of global polynomials with Gaussian quadrature collocation points is known to provide accurate approximations that converge exponentially for problems with smooth solutions. The Gauss pseudospectral method is developed by Benson in an effort to improve the costate estimation of the Legendre pseudospectral method. The Gauss pseudospectral method is originally formulated for optimal

control problems involving integral dynamic constraints, but is later adapted for use with the more common differential dynamic constraints. A key difference between the Gauss and Legendre methods is the choice of discrete points used in the NLP formulation. In this chapter, the open-loop trajectory optimization is solved by the Gauss pseudospectral method.

6.2.2 Feedback Trajectory Control

Under the optimal continuous control inputs, the gripper should track the open-loop trajectory to approach the target. However, the errors between Eqs. (6.9) and (6.10) may cause that the gripper doesn't approach the target. Also, the optimal open-loop trajectory is sensitive to errors in the initial state, actuator errors and external disturbances. Therefore the open-loop trajectory should be implemented with a feedback controller to achieve efficient closed-loop performance. A proven approach for providing feedback control around time-varying reference trajectories is receding-horizon control, which linearizes the system model and solves a linear optimal control problem over a future finite horizon with the initial state equal to the current state [18]. An efficient approach of implementing receding-horizon control is the pseudospectral methods [19]. Another proven technique is to track the open-loop trajectories by formulating the discretized problem as a quadratic programming problem, for which analytical solutions are available. This approach has the following advantages: less memory is required to obtain solutions and availability of closed-form solutions (i.e., eliminating the need to solve a large system of linear equations at each sample time).

In this chapter, a new and more efficient adaptive method is used for control design of the approach stage of TSR. First, the nonlinear trajectory model can be transformed to a linear and time-varying model by linearizing it along the planned reference trajectory. The linear time-varying trajectory model is then converted into the linear time-invariant system by designing the virtual control inputs and separating the small time-varying elements of the state matrix. The linear quadratic regulator is then used, and the actual control inputs are derived from the adaptive control theory. Compared with the previous methods, this approach is much simpler. We must note that this method can only be applied to a state matrix with small time-varying elements.

Along the reference trajectory, the linear time-varying model can be linearized as:

$$\delta\dot{\boldsymbol{X}} = \boldsymbol{A}(t)\delta\boldsymbol{X} + \boldsymbol{B}(t)\delta\boldsymbol{U} \tag{6.16}$$

$$\delta \boldsymbol{X}(t) = \boldsymbol{X}(t) - \boldsymbol{X}_r(t) \tag{6.17}$$

where $\delta \boldsymbol{X}$ are the perturbed state variables, $\delta \boldsymbol{U}$ the perturbed controls, and $\boldsymbol{X}_r$ the reference states. $\boldsymbol{A}$ and $\boldsymbol{B}$ are the system state and control influence matrices.

$$\boldsymbol{A}(t) = \begin{bmatrix}
0 & 1 & 0 & 0 & 0 & 0 & 0 & 0 & 0 & 0 & 0 & 0 \\
\left.\frac{\partial a_{sx}}{\partial x_s}\right| & 0 & \left.\frac{\partial a_{sx}}{\partial \gamma_s}\right| & 0 & \left.\frac{\partial a_{sx}}{\partial z_s}\right| & 2\omega & \left.\frac{\partial a_{sx}}{\partial x_p}\right| & 0 & \left.\frac{\partial a_{sx}}{\partial \gamma_p}\right| & 0 & \left.\frac{\partial a_{sx}}{\partial z_p}\right| & 0 \\
0 & 0 & 0 & 1 & 0 & 0 & 0 & 0 & 0 & 0 & 0 & 0 \\
\left.\frac{\partial a_{s\gamma}}{\partial x_s}\right| & 0 & \left.\frac{\partial a_{s\gamma}}{\partial \gamma_s}\right| - \omega^2 & 0 & \left.\frac{\partial a_{s\gamma}}{\partial z_s}\right| & 0 & \left.\frac{\partial a_{s\gamma}}{\partial x_p}\right| & 0 & \left.\frac{\partial a_{s\gamma}}{\partial \gamma_p}\right| & 0 & \left.\frac{\partial a_{s\gamma}}{\partial z_p}\right| & 0 \\
0 & 0 & 0 & 0 & 0 & 1 & 0 & 0 & 0 & 0 & 0 & 0 \\
\left.\frac{\partial a_{sz}}{\partial x_s}\right| & -2\omega & \left.\frac{\partial a_{sz}}{\partial \gamma_s}\right| & 0 & \left.\frac{\partial a_{sz}}{\partial z_s}\right| + 3\omega^2 & 0 & \left.\frac{\partial a_{sz}}{\partial x_p}\right| & 0 & \left.\frac{\partial a_{sz}}{\partial \gamma_p}\right| & 0 & \left.\frac{\partial a_{sz}}{\partial z_p}\right| & 0 \\
0 & 0 & 0 & 0 & 0 & 0 & 0 & 1 & 0 & 0 & 0 & 0 \\
\left.\frac{\partial a_{px}}{\partial x_s}\right| & 0 & \left.\frac{\partial a_{px}}{\partial \gamma_s}\right| & 0 & \left.\frac{\partial a_{px}}{\partial z_s}\right| & 2\omega & \left.\frac{\partial a_{px}}{\partial x_p}\right| & 0 & \left.\frac{\partial a_{px}}{\partial \gamma_p}\right| & 0 & \left.\frac{\partial a_{px}}{\partial z_p}\right| & 0 \\
0 & 0 & 0 & 0 & 0 & 0 & 0 & 0 & 0 & 1 & 0 & 0 \\
\left.\frac{\partial a_{p\gamma}}{\partial x_s}\right| & 0 & \left.\frac{\partial a_{p\gamma}}{\partial \gamma_s}\right| - \omega^2 & 0 & \left.\frac{\partial a_{p\gamma}}{\partial z_s}\right| & 0 & \left.\frac{\partial a_{p\gamma}}{\partial x_p}\right| & 0 & \left.\frac{\partial a_{p\gamma}}{\partial \gamma_p}\right| & 0 & \left.\frac{\partial a_{p\gamma}}{\partial z_p}\right| & 0 \\
0 & 0 & 0 & 0 & 0 & 0 & 0 & 0 & 0 & 0 & 0 & 1 \\
\left.\frac{\partial a_{pz}}{\partial x_s}\right| & -2\omega & \left.\frac{\partial a_{pz}}{\partial \gamma_s}\right| & 0 & \left.\frac{\partial a_{pz}}{\partial z_s}\right| + 3\omega^2 & 0 & \left.\frac{\partial a_{pz}}{\partial x_p}\right| & 0 & \left.\frac{\partial a_{pz}}{\partial \gamma_p}\right| & 0 & \left.\frac{\partial a_{pz}}{\partial z_p}\right| & 0
\end{bmatrix}$$

$$\boldsymbol{B}(t) = \begin{bmatrix}
0 & \left.\frac{\partial a_{sx}}{\partial T}\right| & 0 & \left.\frac{\partial a_{s\gamma}}{\partial T}\right| & 0 & \left.\frac{\partial a_{sz}}{\partial T}\right| & 0 & \left.\frac{\partial a_{px}}{\partial T}\right| & 0 & \left.\frac{\partial a_{p\gamma}}{\partial T}\right| & 0 & \left.\frac{\partial a_{pz}}{\partial T}\right| \\
0 & \left.\frac{\partial a_{sx}}{\partial F_\gamma}\right| & 0 & \left.\frac{\partial a_{s\gamma}}{\partial F_\gamma}\right| & 0 & \left.\frac{\partial a_{sz}}{\partial F_\gamma}\right| & 0 & 0 & 0 & 0 & 0 & 0 \\
0 & \left.\frac{\partial a_{sx}}{\partial F_z}\right| & 0 & \left.\frac{\partial a_{s\gamma}}{\partial F_z}\right| & 0 & \left.\frac{\partial a_{sz}}{\partial F_z}\right| & 0 & 0 & 0 & 0 & 0 & 0
\end{bmatrix}^{\mathrm{T}}$$

where $\left.\frac{\partial a}{\partial v}\right|$ is the partial derivative of a to v on the reference trajectory $\boldsymbol{X}_r(t)$, a should be a_{sx}, a_{sy}, a_{sz}, a_{px}, a_{py}, a_{pz}, and v should be x_s, γ_s, z_s, x_p, γ_p, z_p, T, F_γ, F_z. $\left.\frac{\partial a}{\partial v}\right|$ is time-varying and significantly less than 1.

The influence of T_{tp} to the platform is much smaller because of the mass. Compared with T_{tpr}, the influence of δT is much smaller, which can be neglected in the feedback control. The model can then be simplified as

$$\begin{cases} \delta\dot{\boldsymbol{X}}_s = (\boldsymbol{A}_n + \boldsymbol{A}_v(t))\delta\boldsymbol{X}_s + \boldsymbol{\nu} \\ \boldsymbol{\nu} = \boldsymbol{B}_s(t)\delta\boldsymbol{U} \end{cases} \tag{6.18}$$

where $\delta\boldsymbol{X}_s = [\delta x_s, \delta\dot{x}_s, \delta\gamma_s, \delta\dot{\gamma}_s, \delta z_s, \delta\dot{z}_s]^{\mathrm{T}}$ are the system state variables, $\boldsymbol{\nu}$ is the virtual control input, $\boldsymbol{A}_n$ is a constant matrix comprising 1 and 0, and $\boldsymbol{A}_v$ is a time-varying matrix and should be considered as the uncertainty of $\boldsymbol{A}_n$.

The quadratic performance index is given as:

$$\delta J = \int_{t_0}^{t_f} \left(\delta\boldsymbol{X}_s{}^{\mathrm{T}}\boldsymbol{Q}\delta\boldsymbol{X}_s + \delta\boldsymbol{\nu}^{\mathrm{T}}\boldsymbol{R}\delta\boldsymbol{\nu}\right) dt \tag{6.19}$$

The optimal law using LQR can be obtained:

$$\boldsymbol{\nu} = -\boldsymbol{R}^{-1}\boldsymbol{P}\delta\boldsymbol{X}_s(t) \tag{6.20}$$

where $\boldsymbol{P}$ is the positive-definite solution to the Algebraic Riccati equation:

$$\boldsymbol{P}\boldsymbol{A}_{\mathbf{n}} + \boldsymbol{A}_{\mathbf{n}}^{\mathrm{T}}\boldsymbol{P} - \boldsymbol{P}\boldsymbol{R}^{-1}\boldsymbol{P} + \boldsymbol{Q} = 0 \tag{6.21}$$

Also, $\boldsymbol{B}_s(t)$ should be expressed as $\boldsymbol{B}_s(\boldsymbol{X})$ for the adaptive control. The actual control input can then be expressed as:

$$\delta\boldsymbol{U} = \boldsymbol{B}_s^{-1}(\boldsymbol{X})\boldsymbol{\nu} = -\boldsymbol{B}_s^{-1}(\boldsymbol{X})\boldsymbol{R}^{-1}\boldsymbol{P}\delta\boldsymbol{X}_s(t) \tag{6.22}$$

6.2.3 Feedback Attitude Control

The attitude control of the gripper of the TSR is almost the same as that of the traditional satellite, except that the former always has an interference of tether tension, which can be suppressed by the reaction wheel and the thrusters.

The attitude angle is small in the approach stage, and the attitude model can be shown as follows:

$$\dot{\boldsymbol{X}}_a = \boldsymbol{A}_a\boldsymbol{X}_a + \boldsymbol{B}_a\boldsymbol{U}_a + (\boldsymbol{B}_{at}\boldsymbol{T}_t + \boldsymbol{B}_{ad}\boldsymbol{T}_d) \tag{6.23}$$

where $\boldsymbol{X}_a = \left[\omega_x, \omega_y, \omega_z, \phi, \theta, \psi\right]^{\mathrm{T}}$ are the system state variables, $\boldsymbol{U}_a = \left[-\dot{h}_x, T_{cz}, T_{cy}\right]^{\mathrm{T}}$ are the system control variables, and the actuator of $\dot{h}_x$ is the reaction wheel.

The quadratic performance index is represented as:

$$J_a = \int_{t_0}^{t_f} \left(\boldsymbol{X}_a{}^{\mathrm{T}}\boldsymbol{Q}_a\boldsymbol{X}_a + \boldsymbol{U}_a^{\mathrm{T}}\boldsymbol{R}_a\boldsymbol{U}_a\right) dt \tag{6.24}$$

By using LQR, the optimal attitude control can be obtained:

$$\boldsymbol{U}_a = -\boldsymbol{R}_a^{-1}\boldsymbol{B}_a^{\mathrm{T}}\boldsymbol{P}_a\boldsymbol{X}_a(t) \tag{6.25}$$

where $\boldsymbol{P}_a$ is the positive-definite solution to the Algebraic Riccati equation:

$$\boldsymbol{P}_a\boldsymbol{A}_{\mathbf{a}} + \boldsymbol{A}_{\mathbf{a}}^{\mathrm{T}}\boldsymbol{P}_a - \boldsymbol{P}_a\boldsymbol{B}_a\boldsymbol{R}_a^{-1}\boldsymbol{B}_a^{\mathrm{T}}\boldsymbol{P}_a + \boldsymbol{Q}_a = 0 \tag{6.26}$$

Additionally, to reduce the propellant, a control dead zone of the pitch and yaw channels is designed for the small attitude errors.

6.3 NUMERICAL SIMULATION

A representative approach stage has been selected to demonstrate the performance of the proposed methods. The target is assumed to be in an orbit with a radius of 6871 km, and the orbit angular velocity is 0.0011 rad/s. The key parameters are given in Table 6.2.

To prevent the tether from being slack, the tension must be positive. Considering the characteristics of the system, the open-loop trajectory can be determined by using Eq. (6.27).

$$\begin{cases} \boldsymbol{U}_{\min} = [0.015N, -0.1N, -0.1N]^{\mathrm{T}} \\ \boldsymbol{U}_{\max} = [0.3N, 0.1N, 0.1N]^{\mathrm{T}} \end{cases} \tag{6.27}$$

The Gauss pseudospectral method is used with the initial guess of $\boldsymbol{X}_{t_0}$ and $\boldsymbol{X}_{t_f}$ with zero control inputs. The corresponding optimal continuous control force via Lagrange interpolation is shown in Fig. 6.5. Fig. 6.5 shows the comparison of T_{tp} and $T_{1,0}$. The maximum and minimum deployment

Table 6.2 Sample task parameters

System	Parameters	Value
Platform	Mass	1000 kg
	Initial position/velocity	[−200 m, 5 m, 5 m]/[0.05 m/s, 0 m/s, 0 m/s]
Tether	Arm of tension	[0 m, −0.28 m, 0.28 m]
	Tether longitudinal stiffness	1.0398×10^5 N
	Tether density	4.5 kg/km
Gripper	Mass	10 kg
	Moment of inertia	diag[0.0945,0.2266,0.2441] kg m^2
	Initial position/velocity	[−198 m, 5 m, 5 m], [1 m/s, 0 m/s, 0 m/s]
	Terminal position/velocity	[0 m, 0 m, 0 m]/[0.05 m/s, 0 m/s, 0 m/s]
	Initial attitude/angular velocity	[0 degree, 0 degree, 0 degree]/[0 degree/s, 0 degree/s, 0 degree/s]
	Arms of couple (y, z)	0.25 m, 0.25 m

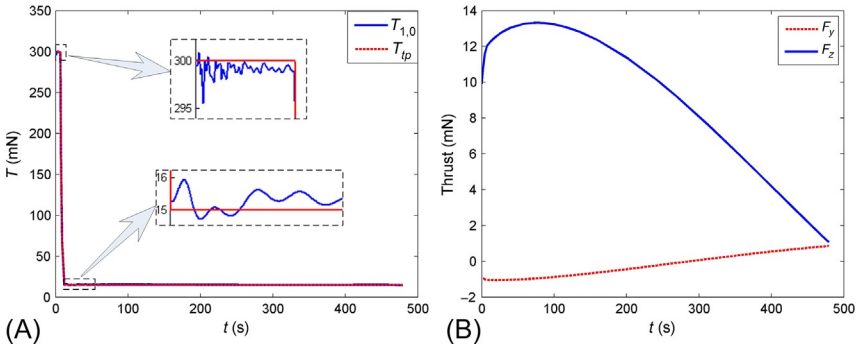

Fig. 6.5 Optimal open-loop control inputs: (A) the comparison of T_{tp} and $T_{1,0}$ and (B) the thrusts of the gripper.

forces (T_{tp}) are 300 and 15 mN. The actual tether tension $T_{1,0}$ can track T_{tp}. The maximum tracking error is less than 5 mN. The thrusts of the gripper are shown in Fig. 6.5B. The thrusts are less than 16 mN. For the deviation out of the orbital plane, F_z is much larger which means more propellant consumption. Under the optimal continuous control inputs, the gripper should approach the target along the open-loop optimal trajectory.

Even though the numerical methods can be used to generate the optimal control profiles, it is desirable to implement such solutions with an appropriate feedback strategy such that closed-loop stability can be demonstrated. As a result, the open-loop optimal control inputs could be stored, or even determined just before initiating the control actions, and then a feedback controller can be used to track the desired states. Because the design of the open-loop optimal control does not include the influence of attitude, the controller can be validated in the model, which contains the dynamic coupling between the trajectory model and the attitude model (Eqs. 6.1 and 6.9).

The weighting matrices are selected as $\mathbf{Q} = 10\mathbf{I}_{6\times6}$, $\mathbf{R} = 5\mathbf{I}_{3\times3}$, $\mathbf{Q}_a = \mathbf{I}_{6\times6}$, and $\mathbf{R}_a = \text{diag}[20,\ 2000,\ 2000]$. The attitude control dead zone of the pitch and yaw channels is selected as [−5 degree, 5 degree].

Figs. 6.6 and 6.7 show the numerical results of the representative approach stage. Fig. 6.6 is the states of the gripper in the approach stage. x_{sr}, y_{sr}, z_{sr}, $\dot{x}_{sr}$, $\dot{y}_{sr}$, and $\dot{z}_{sr}$ are the open-loop trajectory instruction. x_s, y_s, z_s, $\dot{x}_s$, $\dot{y}_s$, and $\dot{z}_s$ are the actual states of the gripper. ϕ, θ, and ψ are the actual attitude angles. The actual states can track the desired states of the open-loop optimal trajectory. The maximum errors of positions are less than 0.1 m. The maximum errors of velocities are less than 0.01 m/s. The angles θ and ψ are between −4 and 4 degree under the thrusters. The roll angle ϕ

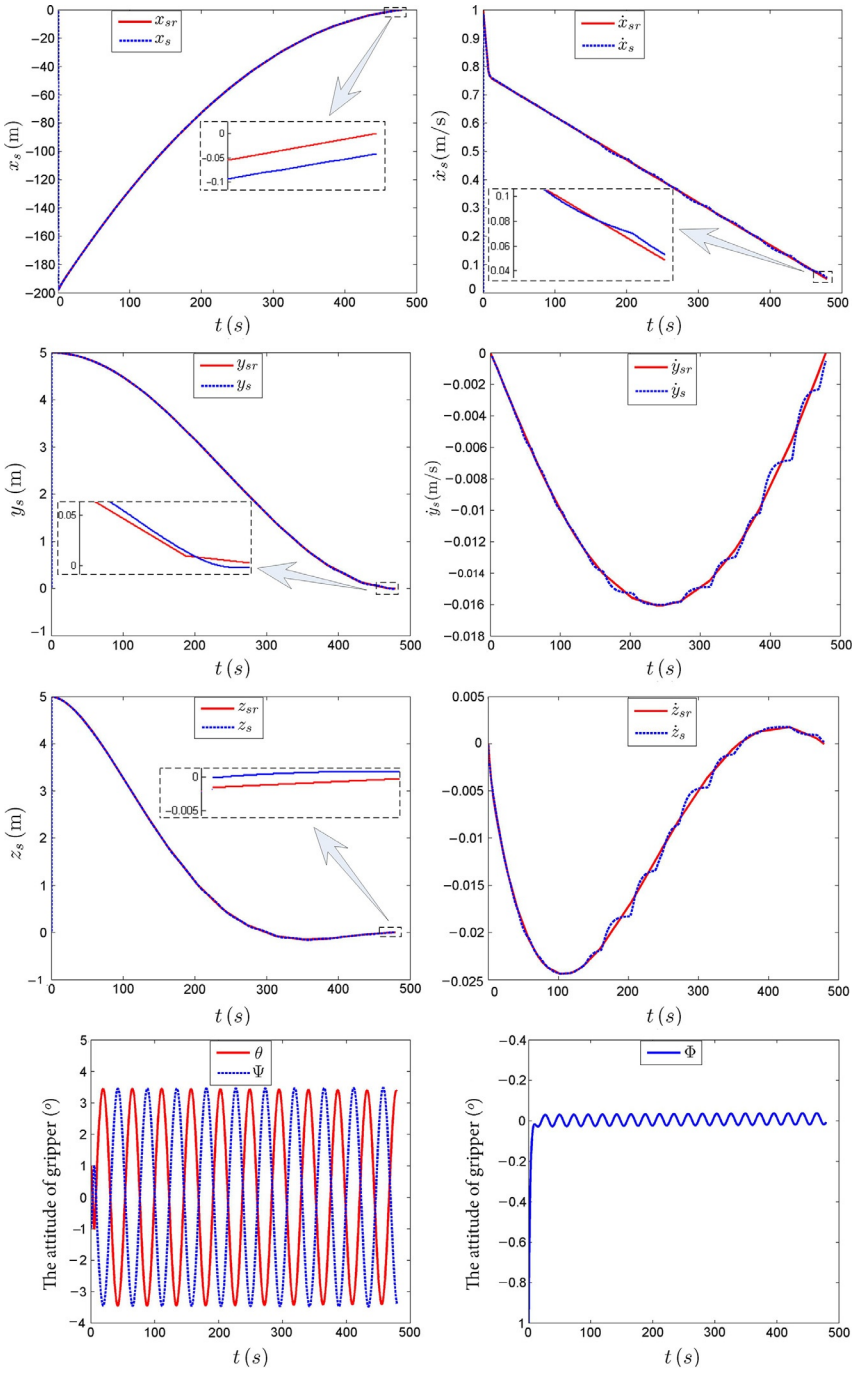

Fig. 6.6 States of gripper in a representative approach stage.

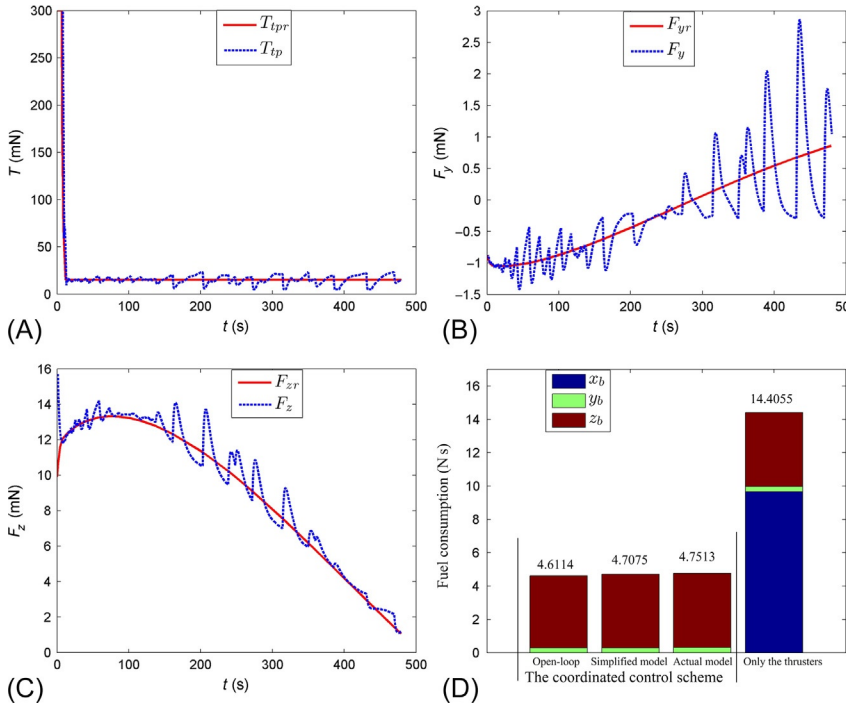

Fig. 6.7 Control inputs in a representative approach stage.

is between −0.1 and 0.1 degree under the control moment of the reaction wheel. Fig. 6.7 shows the control inputs. T_{tpr}, F_{yr}, and F_{zr} are the open-loop control inputs. T_{tp}, F_y, and F_z are the actual feedback control inputs. T_{tp} is between 5 and 300 mN. F_y is between −1.5 and 3 mN. F_z is between 0 and 16 mN. Fig. 6.7D shows the fuel consumptions. x_b, y_b, and z_b indicate the fuel consumptions of the gripper along $\boldsymbol{s}_b, \boldsymbol{y}_b, \boldsymbol{z}_b$. The fuel consumption is 4.6114 N s for the open-loop optimal control. In the simulation with simplified model and actual model, the fuel consumption reaches 4.7075 and 4.7513 N s, respectively. However, without the coordinated control scheme, the fuel consumption is 14.4055 N s.

The closed-loop simulations show that the coordinated approach control scheme is effective, even under the initial states perturbations, the actuator characteristics, and the sensor errors. However, there still exist several questions including how to select the suitable sensors to observe all of the system state variables, how to control the required tether tension, and whether the system still performs as well in the presence of additional uncertainties. Nevertheless, the results presented suggest that the control strategy of TSR is capable of achieving rendezvous in the on-orbit capture task.

REFERENCES

[1] X.D. Du, B. Liang, W.F. Xu, Y. Qiu, Pose measurement of large noncooperative satellite based on collaborative cameras, Acta Astronaut. 68 (2011) 2047–2065.
[2] N.D. Doulamis, Coupled multi-object tracking and labeling for vehicle trajectory estimation and matching, Multimed. Tools Appl. 50 (2010) 173–198.
[3] J.K. Thienel, J.M. VanEepoel, R.M. Sanner, Accurate state estimation and tracking of a non-cooperative target vehicle, in: AIAA Guidance, Navigation, and Control Conference and Exhibit, Keystone, Colorado, August 21–24, 2006.
[4] J.A. Carroll, Tether applications in space transportation, Acta Astronaut. 13 (4) (1986) 165–174.
[5] J.A. Carroll, Preliminary design for a 1 km/sec tether transport facility, in: NASA Office of Aeronautics and Space Technology, Third Annual Advanced Propulsion Workshop, January 1992.
[6] D.G. Stuart, Guidance and control for cooperative tether-mediated orbital rendezvous, J. Guid. Control. Dyn. 13 (6) (1990) 1102–1113.
[7] C. Blanksby, P. Trivailo, Assessment of actuation methods for manipulating tip position of long tethers, space technology, Space Eng. Telecommun. Syst. Eng. Control 20 (1) (2001) 31–40.
[8] J. Westerhoff, Active control for MXER tether rendezvous maneuvers, in: AIAA-2003-5218, 2003.
[9] C. Blanksby, P. Trivailo, H.A. Fujii, In-plane payload capture using tethers, Acta Astronaut. 57 (10) (2005) 772–787.
[10] P. Williams, Spacecraft rendezvous on small relative inclination orbits using tethers, J. Spacecr. Rocket. 42 (6) (2005) 1047–1060.
[11] P. Williams, In-plane payload capture with an elastic tether, J. Guid. Control. Dyn. 29 (4) (2006) 810–821.
[12] P. Williams, Heating and modeling effects in tethered aerocapture missions, J. Guid. Control. Dyn. 26 (4) (2003) 643–654.
[13] H. Wen, D.P. Jin, H.Y. Hu, Advances in dynamics and control of tethered satellite systems, Acta Mech. Sin. 24 (3) (2008) 229–241.
[14] M. Krupa, W. Poth, M. Schagerl, et al., Modeling, dynamics and control of tethered satellite systems, Nonlinear Dyn. 43 (2006) 73–96.
[15] A. Steindl, H. Troger, Optimal control of deployment of a tethered subsatellite, Nonlinear Dyn. 31 (2003) 257–274.
[16] K.K. Mankala, S.K. Agrawal, Dynamic modeling and simulation of impact in tether net/gripper systems, Multibody Sys.Dyn. 11 (3) (2004) 235–250.
[17] N. Yuya, S. Fumiki, N. Shinichi, Guidance and control of "tethered retriever" with collaborative tension-thruster control for future on-orbit service missions, in: The 8th International Symposium on Artificial Intelligence: Robotics and Automation in Space-ISAIRAS, Munich, Germany, September 5–8, 2005.
[18] D. Garg, M. Patterson, W.H. William, et al., A unified framework for the numerical solution of optimal control problems using pseudospectral methods, Automatica 46 (2010) 1843–1851.
[19] P. Lu, Regulation about time-varying trajectories: precision entry guidance illustrated, J. Guid. Control. Dyn. 6 (22) (1999) 784–790.